Performance Enhancement and Evaluation of a Vector Tracking Receiver using Adaptive Tracking Loops

Ning Gao , Xiyuan Chen * , Zhe Yan , Zhiyuan Jiao

Posted Date: 28 December 2023

doi: 10.20944/preprints202312.1948.v1

Keywords: vector tracking; tracking loop; nonlinear Kalman filter; GNSS software-defined receiver

Article

Performance Enhancement and Evaluation of a Vector Tracking Receiver Using Adaptive Tracking Loops

Ning Gao [1], Xiyuan Chen [1,*], Zhe Yan [1,2] and Zhiyuan Jiao [1]

[1] School of Instrument Science and Engineering, Southeast University, Nanjing 210096, China
[2] Department of Computer Science, University of Helsinki, Helsinki 00014, Finland
* Correspondence: chxiyuan@seu.edu.cn

Abstract: The traditional receiver employs scalar tracking loops, resulting in degraded navigation performance in weak signal and high dynamic scenarios. An innovative design of a vector tracking receiver based on nonlinear Kalman filter (KF) tracking loops is proposed in this paper, which combines the strengths of both vector tracking and KF tracking loops. Firstly, a comprehensive description of the vector tracking receiver model is presented, and unscented Kalman filter (UKF) is applied to nonlinear tracking loop. Secondly, to enhance the stability and robustness of the KF tracking loop, we introduce square root filtering and an adaptive mechanism. The tracking loop based on square root UKF (SRUKF) can dynamically adjust its filtering parameters based on signal noise and feedback Doppler error. Finally, the proposed method is implemented on a software-defined receiver (SDR), and the field vehicle experiment demonstrates the superiority of this method over other receivers in complex dynamic environments.

Keywords: vector tracking; tracking loop; nonlinear Kalman filter; GNSS software-defined receiver

1. Introduction

Global satellite navigation system (GNSS) has become one of the most widely used navigation systems because of its advantages of high precision, all-weather, continuous positioning, extensive coverage, convenience and flexibility [1,2]. As the demand for navigation performance rises, GNSS will inevitably be affected by the specific application scenario and the movement characteristics of the carrier, such as low signal carrier-to-noise ratio (C/N_0) environments (e.g., signal blocking and interference) and high dynamic motion [3–6].

GNSS receivers acquire position, velocity, and time (PVT) information by tracking satellite broadcast signals in real time, demodulating navigation messages, and acquiring pseudo-range, Doppler frequency, and other observation information. Therefore, the tracking loop accuracy of the receiver directly determines the PVT accuracy. Consequently, the accuracy of the receiver's tracking loop is a direct determinant of the precision in PVT estimation. Traditional GNSS receivers usually adopt scalar tracking loops (STL) to track each satellite independently using individual pre-assigned channel, and the signal processing among each channel is independent of each other. This tracking mode is simple to implement, without interference and pollution between channels [7]. However, it ignores the inherent correlation of GNSS tracking loops to the receiver's PVT information, so information cannot be shared between each channel. In contrast, vector tracking loops (VTL) interlink the tracking loops and navigation solutions of diverse channels, facilitating the exchange of information between them, which has been widely concerned in recent years [8–11]. Compared with the STL, the VTL exploits and makes full use of the redundant information of different satellite signals and the intrinsic coupling between signal tracking and navigation solution, and its advantages mainly include: 1) with the aid of navigation information, VTL mitigates the dynamic stress on the tracking loop, enhancing the dynamic performance of the receiver; 2) VTL excels in balance the correlation of information between receiver signal channels, showcasing superior performance in

 doi:10.20944/preprints202312.1948.v1

scenarios involving weak signal tracking and rapid retracking; 3) it also exhibits superior anti-interference performance.

In general, STL tracks satellite signals by using conventional tracking loops (CTL) based on classical control theory, encompassing phase locking loops (PLL), frequency locking loops (FLL), and delay locking loops (DLL). The characteristics of CTL are determined by noise bandwidth and loop order. Notably, the selection of noise bandwidth involves a delicate trade-off between achieving low noise and maintaining high dynamic performance. Within the VTL, the dynamic stress of the loop filter is significantly alleviated through the incorporation of feedback information, which allows the tracking loop to concentrate exclusively on thermal noise, crystal frequency error, and dynamic residual [12,13]. Consequently, there is an opportunity to diminish the loop bandwidth, simultaneously improving tracking accuracy. It is important to note, however, that the loop bandwidth remains constrained by crystal frequency errors and feedback errors. In complex environments, signals may be affected by high dynamics, shadows, strong attenuation, multipath effects, or ionospheric scintillation, in which scenarios the performance of fixed-bandwidth tracking loop will deteriorate or even become ineffective. Therefore, the adaptive loop tracking (ALT) technology has garnered substantial research attention due to its ability to dynamically adjust the loop bandwidth in response to the varying noise levels encountered in different scenarios [14–16]. The contribution of the [17] derives the Doppler aiding error due to the uncertainty of the navigation error in the GPS/INS ultra-tight integration, and designs a PLL loop filter whose noise bandwidth can be adaptively adjustable according to the performance of the integrated navigation and the C/N_0 of the GPS signal. In the [18], the adaptive scalar tracking techniques used by the fast adaptive bandwidth (FAB), the fuzzy logic (FL), and the loop-bandwidth control algorithm (LBCA) are delineated. A meticulous analysis of the tracking performance and time complexity of each method is conducted. These techniques dynamically adjust the loop bandwidth based on predefined discriminant criteria, thereby optimizing tracking performance for different scenarios. However, the adaptability of these adjustments is contingent upon specific discriminant criteria and thresholds.

Kalman filter (KF) based on optimal estimation theory stands out as an alternative method for dynamically adjusting loop noise bandwidth, gaining substantial attention in recent years owing to its superior performance in comparison to CTL [19,20]. The KF-based tracking loops replace conventional loop filters by estimating the loop parameters (e.g., carrier phase, Doppler frequency, and code phase) as state variables. Recherche process noise covariance **Q** and measurement noise covariance **R** enable KF to optimally adjust its gain coefficient in time-varying scenarios to achieve minimum mean square error (MMSE) criterion. Therefore, the real-time estimation and adjustment of **Q** and **R** play a crucial role in determining the filtering accuracy for time-varying scenarios. Numerous studies have delved into methods for adjusting KF parameters. Tang et al. [21,22] analyzes the relationship between the equivalent bandwidth of KF-based tracking loop and noise covariance, subsequently deducing the criteria for parameter setting. In [23], variational Bayesian (VB) theory is employed to dynamically estimate the measurement noise matrix, which improves the tracking accuracy in high dynamic scenes. Moreover, the process noise matrix can be adaptively tuned based on the characteristics of the crystal oscillator and receiver dynamics in STL [24]. However, there is a scarcity of research regarding the implementation of KF-based tracking loops in the VTL.

According to the different measurement information used, the signal tracking based on KF usually has two forms: one structure uses the output of traditional discriminator as measurement information and is implemented by linear KF; the other structure is measured by coherent integration results and implemented by nonlinear KF. Unfortunately, the loop discriminator introduces nonlinear noise in highly dynamic applications, deviating from the Gaussian white noise (GWN) property, thereby constraining the estimation accuracy. Therefore, in order to improve the tracking accuracy and dynamic range, the entire discriminator and tracking loop filter are replaced by a nonlinear tracking filter. In this case, the measurement is the outcome of the correlation between the input signal and the local signal, showcasing a nonlinear relationship with the estimated vector. Therefore, the application of a nonlinear filtering method is essential to achieve improved accuracy. Tang et al. [25] provides a comprehensive analysis of the practical implementation architecture for

 doi:10.20944/preprints202312.1948.v1

tracking loops based on extended Kalman filters (EKF). Zeng et al. [26] compared the EKF-based tracking loop of GPS receiver with the CTL, demonstrating that the EKF-based tracking loop excels in both high dynamic and tracking accuracy. Nevertheless, the EKF algorithm is a sub-optimal filtering algorithm based on nonlinear functionalization and adopts approximation or neglect method for higher order terms to solve nonlinear problems [27]. In the case of strong nonlinearity, it may result in a significant estimation error and even lead to filter divergence. Moreover, in practical applications, the computational complexity of obtaining the derivative of the Jacobian matrix for nonlinear functions is substantial.

To address the challenges inherent in the EKF, alternative methods such as the particle filter (PF) and unscented Kalman filter (UKF) have been proposed for nonlinear filtering problems [28,29]. PF, a recursive Bayesian filtering (BF) method, employs random samples to represent the posterior probability distribution of system state variables, overcoming certain limitations of EKF. However, PF requires a substantial number of particles to achieve high-precision estimation, resulting in a significant computational burden, particularly in scenarios with a high update rate for the tracking loop, which makes it difficult to operate in real time. The UKF is a method for approximating nonlinear distributions using a deterministic sampling strategy, which relies on the Unscented Transform (UT) and maintains the framework of a linear KF. In contrast to PF, the UKF replaces random sampling with deterministic sampling, while maintaining comparable computational complexity to the EKF. However, the performance is better than EKF, making it a widely adopted choice for nonlinear filtering [30,31].

Inspired by the above research, a vector tracking receiver has been developed that leverages an adaptive square root UKF (ASRUKF) tracking loops to enhance the precision and robustness of GNSS receivers in complex dynamic environments. The primary contributions of this research are as follows:

1) A vector receiver model based on a nonlinear tracking loop is designed, with comprehensive details provided on its implementation. The discriminator and traditional filter in the tracking loop are substituted with the UKF, and the Doppler feedback calculated by the navigation solution is incorporated into the loop filter. It accomplishes not only the loop tracking assistance by Doppler frequency but also establishes indirect connections between each channel, fostering mutual assistance.
2) To enhance the stability and robustness of the tracking loop, the square root filter is introduced into UKF. Additionally, the measurement noise covariance and process noise covariance of UKF are adjusted adaptively according to the signal C/N_0 and feedback information error, respectively. This adaptive adjustment enables real-time modification of the loop noise bandwidth, consequently enhancing the performance of the tracking loop.
3) The effectiveness of the proposed method was verified through field vehicle experiments conducted on urban roads. Software-defined receiver (SDR) with different structures were developed to facilitate performance comparison and analysis. The results affirm that the KF-based VTL offers a substantial improvement over the CTL-based VTL, while demonstrating that the tracking accuracy of the UKF-based VTL surpasses that of the EKF-based VTL. Moreover, the ASRUKF-based VTL exhibits further performance improvement in complex dynamic environments.

The structure of this paper is organized as follows. In Section 2, the overall model of the vector tracking receiver is divided into three parts to describe in detail. Section 3 describes the design method of tracking loop based on adaptive square root UKF. In Section 4, the proposed VTL architecture is evaluated in a practical scenario and its performance is compared and analyzed within the SDR framework. Eventually, the conclusions and prospects are summarized in Section 5.

2. System Model of Vector Tracking

Generally, VTL receiver primarily comprises three components: nonlinear KF-based tracking loop; navigation solution module, and vector feedback calculation. The structure block diagram is illustrated in Figure 1.

Preprints (www.preprints.org) | NOT PEER-REVIEWED | Posted: 28 December 2023 doi:10.20944/preprints202312.1948.v1

The GNSS intermediate frequency (IF) signal is correlated with the local signal to obtain the I/Q components, which are then processed by the loop filter to generate pseudo-range and Doppler frequency information as the measurement of the navigation solution. After the navigation filter estimates the receiver's PVT information, the satellite line-of-sight (LOS) vector for each channel is calculated by incorporating the satellite ephemeris information. Then, the feedback code phase and Doppler frequency are calculated and combined with the loop filtering results to adjust the local numerically controlled oscillator (NCO), thereby establishing a closed-loop system. The EKF is typically employed in the navigation solution module, resulting in the development of a cascaded vector tracking structure with the nonlinear KF-based tracking loop. This proposed structure not only lowers the update rate of the navigation filter but also reduces computational complexity and enhances ease of implementation.

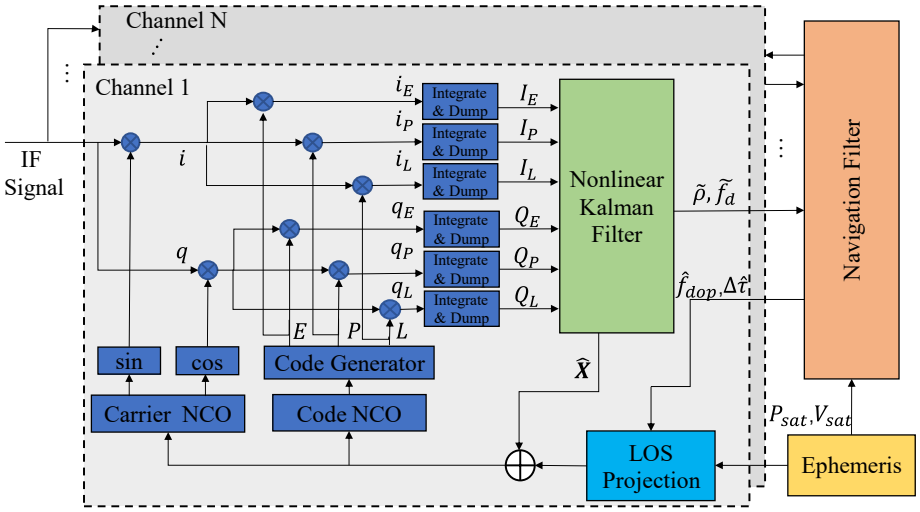

Figure 1. Structure block diagram of proposed VTL.

2.1. Nonlinear KF-based Tracking Loop

Given that the discriminator is substituted with a loop filter, the I/Q information is utilized directly as the measurement for KF. The state vector to be estimated comprises the following components: signal amplitude A, code phase error $\Delta\tau$, carrier phase error $\Delta\theta$, carrier frequency error Δf, and carrier frequency rate error $\Delta\alpha$. The system model can be formulated as follows:

$$\begin{bmatrix} \dot{A} \\ \Delta\dot{\tau} \\ \Delta\dot{\theta} \\ \Delta\dot{f} \\ \Delta\dot{\alpha} \end{bmatrix} = \begin{bmatrix} 0 & 0 & 0 & 0 & 0 \\ 0 & 0 & 0 & \beta & 0 \\ 0 & 0 & 0 & 2\pi & 0 \\ 0 & 0 & 0 & 0 & 1 \\ 0 & 0 & 0 & 0 & 0 \end{bmatrix} \bullet \begin{bmatrix} A \\ \Delta\tau \\ \Delta\theta \\ \Delta f \\ \Delta\alpha \end{bmatrix} + \begin{bmatrix} 1 & 0 & 0 & 0 & 0 \\ 0 & 1 & \beta & 0 & 0 \\ 0 & 0 & 1 & 0 & 0 \\ 0 & 0 & 0 & 1 & 0 \\ 0 & 0 & 0 & 0 & 1 \end{bmatrix} \bullet \begin{bmatrix} w_A \\ w_\tau \\ w_\theta \\ w_f \\ w_\alpha \end{bmatrix} \tag{1}$$

where the coefficient β is utilized to convert the cycles into chips, enabling unit conversion (e.g., for GPS L1: β=1/1540). The value $w_A, w_\tau, w_\theta, w_f, w_\alpha$ represent the process noises of the signal amplitude, code phase error, clock bias, clock drift and frequency rate error, respectively.

The I/Q correlation values serve as the measurement of the filter, expressed in terms of:

$$\mathbf{Z} = \begin{bmatrix} I_P & I_E & I_L & Q_P & Q_E & Q_L \end{bmatrix}^T \tag{2}$$

The variables I_P, I_E, and I_L represent the 'prompt', 'early', and 'late' correlation results of the In-phase correlator, respectively. Similarly, Q_P, Q_E, and Q_L represent the corresponding correlation results of the Quadrature-phase correlator.

The expression for the output of loop correlation value I/Q has been formulated:

Preprints (www.preprints.org) | NOT PEER-REVIEWED | Posted: 28 December 2023 doi:10.20944/preprints202312.1948.v1

$$I = \frac{A}{2} \bullet D \bullet R\left(\Delta\tau + \xi d\right) \bullet \mathrm{sinc}\left(\pi T_{coh} \Delta f\right) \bullet \cos\left(\overline{\Delta\varphi}\right) + \eta_I$$
$$Q = \frac{A}{2} \bullet D \bullet R\left(\Delta\tau + \xi d\right) \bullet \mathrm{sinc}\left(\pi T_{coh} \Delta f\right) \bullet \sin\left(\overline{\Delta\varphi}\right) + \eta_Q \quad (3)$$

where D is the navigation message, $R(\bullet)$ is the autocorrelation function, T_{coh} is the coherence integration time, represents the duration over which the received signals are integrated to estimate the coherence function. d is the correlator interval. For the early, prompt, and late branches, ξ are -1, 0, and +1 respectively. Additionally, η_I and η_Q represent zero-mean GWN that is independent of the I/Q branches. The average carrier phase error $\overline{\Delta\varphi}$ in the coherent integration time T_{coh} is computed according to the following formula:

$$\overline{\Delta\varphi} = \Delta\theta + \Delta f \frac{T_{coh}}{2} + \Delta\alpha \frac{T_{coh}^2}{6} \quad (4)$$

Note that the Equation **Error! Reference source not found.** signifies a nonlinear relationship between the measurement and the state vector of the tracking loop.

2.2. Nonlinear KF-based Tracking Loop

The VTL employs the EKF instead of the least square (LS) method to fuse pseudo-range and Doppler frequency for calculating the optimal PVT solution. This decision is based on its superior filtering performance and simplified fault detection and isolation capabilities.

The state vector representing the navigation solution is outlined as follows:

$$\mathbf{X}_{nav} = \left[\boldsymbol{\delta}\mathbf{P}_{1\times3} \quad \boldsymbol{\delta}\mathbf{V}_{1\times3} \quad \delta t_b \quad \delta t_d\right]^T \quad (5)$$

where $\delta\mathbf{P} = \left[\delta x \quad \delta y \quad \delta z\right]$ is the errors vector of position in ECEF coordinate system; $\delta\mathbf{V} = \left[\delta v_x \quad \delta v_y \quad \delta v_z\right]$ is the corresponding velocity errors vector. δt_b and δt_d refer to the errors associated with clock bias and drift of receiver.

The system adopts the constant velocity model, thus enabling the expression of the discrete state transition matrix of the system as follows:

$$\mathbf{F}_{nav} = \begin{bmatrix} \mathbf{I}_3 & T_{nav}\mathbf{I}_3 & \mathbf{0}_{6\times2} \\ \mathbf{0}_3 & \mathbf{I}_3 & \\ & & \begin{matrix} 1 & T_{nav} \\ 0 & 1 \end{matrix} \end{bmatrix} \quad (6)$$

where T_{nav} represents the navigation filter update time, $\mathbf{I}_3$ is a three-dimensional identity matrix.

The measurement of the navigation filter consists of the difference between the calculated and estimated pseudo-range, along with the Doppler frequency for each channel:

$$\mathbf{Z}_{nav} = \left[\tilde{\rho}^{(1)} - \hat{\rho}^{(1)}, \cdots, \tilde{\rho}^{(m)} - \hat{\rho}^{(m)}, \tilde{f}_{dop}^{(1)} - \hat{f}_{dop}^{(1)}, \cdots, \tilde{f}_{dop}^{(m)} - \hat{f}_{dop}^{(m)}\right]^T \quad (7)$$

The variables $\tilde{\rho}^{(m)}$ and $\tilde{f}_{dop}^{(m)}$ represent the measured pseudo range and Doppler frequency of channel m respectively, while $\hat{\rho}^{(m)}$ and $\hat{f}_{dop}^{(m)}$ denote the estimated pseudo-range and Doppler frequency correspondingly.

The matrix representing the transfer of measurements is presented below [32]:

Preprints (www.preprints.org) | NOT PEER-REVIEWED | Posted: 28 December 2023 doi:10.20944/preprints202312.1948.v1

$$\mathbf{H}_{nav}=\begin{bmatrix} e_x^1 & e_y^1 & e_z^1 & 0 & 0 & 0 & 1 & 0 \\ \vdots & \vdots & \vdots & \vdots & \vdots & \vdots & \vdots & \vdots \\ e_x^m & e_y^m & e_z^m & 0 & 0 & 0 & 1 & 0 \\ 0 & 0 & 0 & e_x^1 & e_y^1 & e_z^1 & 0 & 1 \\ \vdots & \vdots & \vdots & \vdots & \vdots & \vdots & \vdots & \vdots \\ 0 & 0 & 0 & e_x^m & e_y^m & e_z^m & 0 & 1 \end{bmatrix} \tag{8}$$

where, $\mathbf{e}^m=\begin{bmatrix} e_x^m & e_y^m & e_z^m \end{bmatrix}^T$ is the LOS vector from the receiver to the *m*-th satellite, calculation as follows:

$$\mathbf{e}^m=\frac{\mathbf{p}_s^m-\mathbf{p}_u}{\left\|\mathbf{p}_s^m-\mathbf{p}_u\right\|} \tag{9}$$

where, $\mathbf{p}_u$ and $\mathbf{p}_s^m$ represent the position vectors of the receiver and the *m*-th satellite respectively.

2.3. Nonlinear KF-based Tracking Loop

When the PVT information is estimated by the navigation filter, the carrier and code NCO feedback correction information of each channel can be calculated by combining the satellite ephemeris.

The Doppler frequency estimation of the tracking channel *j* at time *k* can be computed as follows:

$$\hat{f}_{dop,k}^j=\left[t_{d,k}+\mathbf{e}_k^j\cdot(\mathbf{v}_{s,k}^j-\mathbf{v}_{u,k})\right]\cdot\frac{f_{carrier}}{c} \tag{10}$$

where $\mathbf{v}_{u,t}$ and $\mathbf{v}_{s,t}^j$ are the receiver velocity and the velocity of the channel *j* satellite, respectively, while $t_{d,t}$ denotes the clock drift at time *k*. Additionally, $f_{carrier}$ corresponds to the carrier frequency (e.g., for GPS L1 $f_{carrier}=1575.42MHz$), and c signifies the velocity of light (e.g., $c=29979245m/s$).

Combined with the results of the loop filter, the final carrier frequency is:

$$\hat{f}_{carrier,k}^j=f_{IF}+\hat{f}_{dop,k}^j+\mathbf{X}_k^j(4)+\mathbf{X}_k^j(5)\bullet T_{coh} \tag{11}$$

where, f_{IF} is the IF signal of the RF front-end output, and $\mathbf{X}_k^j(n)$ is the *n*-th element of the state vector $\mathbf{X}_k^j$ of tracking loop at time *k*.

As evident from the Equation **Error! Reference source not found.**, the incorporation of Doppler frequency significantly alleviates the dynamic stress of the loop. This not only enhances the dynamic performance of the receiver, but also allows the loop filter to further decrease the noise bandwidth, consequently improving tracking accuracy and sensitivity.

Accordingly, the estimation of code frequency can be calculated directly using a carrier Doppler assisted form:

$$\hat{f}_{code,k}^j=f_{code}\cdot\left(1+\hat{f}_{dop,k}^j\cdot\frac{1}{f_{carrier}}\right) \tag{12}$$

The code phase is computed according to the following procedure:

$$\hat{\tau}_{code,k}^j=\tau_{code,k\text{-}1}^j+\frac{\mathbf{e}_k^j\cdot(\mathbf{p}_{s.k}^j-\mathbf{p}_{u.k})}{\lambda_{chip}}+\mathbf{X}_k^j(2)+\beta\left(\mathbf{X}_k^j(4)\bullet T_{coh}+\frac{\mathbf{X}_k^j(5)}{2}\bullet T_{coh}^2\right) \tag{13}$$

where λ_{chip} is the length of the pseudo-code chip (e.g., for GPS L1 C/A signal: $\lambda_{chip}=1023$).

Furthermore, following the completion of the NCO update, the state vector is reset to zero, thereby initiating the subsequent cycle's state estimation process.

Preprints (www.preprints.org) | NOT PEER-REVIEWED | Posted: 28 December 2023 doi:10.20944/preprints202312.1948.v1

3. Proposed Adaptive SRUKF-based Loop Tracking

The tracking loop filter can be represented by a nonlinear state space model:

$$\begin{cases} \mathbf{X}_k = f\left(\mathbf{X}_{k-1}\right) + \mathbf{W}_{k-1} \\ \mathbf{Z}_k = h\left(\mathbf{X}_k\right) + \mathbf{V}_k \end{cases} \tag{14}$$

where, $\mathbf{X}_k$ denotes the state vector and $\mathbf{Z}_k$ is the measurement vector, while $f(\bullet)$ and $h(\bullet)$ are nonlinear functions of the system and measurement model, respectively. The vectors $\mathbf{W}_{k-1}$ and $\mathbf{V}_k$ correspond to process noise and measurement noise with zero-mean and covariance $\mathbf{Q}_k$ and $\mathbf{R}_k$, respectively.

3.1. Square Root Unscented Kalman Filter

The UKF utilizes sigma points to approximate the functional probability density distribution, thereby facilitating nonlinear filtering. However, the necessity of calculating sigma points at each update, which involves taking the square root of the state covariance matrix, can lead to issues such as computational burden and numerical instability. By integrating the concept of square root filtering within the UKF framework, it is possible to reduce computational complexity and enhance efficiency. This is achieved through direct recursion updating in the form of the square root of the covariance matrix. Moreover, this approach guarantees the non-negativity of the covariance matrix, effectively prevents filter divergence, and fosters the convergence speed and numerical stability of the filter.

The Square Root Unscented Kalman Filter (SRUKF) utilizes *QR* decomposition and *Cholesky* factor update techniques to replace the covariance matrix with its square root, thereby enhancing the efficiency of the filtering iteration. The specific procedural steps are delineated in Table 1.

3.2. Adaptive SRUKF-based Loop Tracking for Vector Tracking

In the VTL, different from STL, the tracking loop can eliminate most of the dynamic stress with the assistance of Doppler frequency. However, this also introduces additional frequency errors due to navigation inaccuracies. Beyond addressing loop thermal noise and receiver crystal error, the tracking loop also tracks the Doppler auxiliary error induced by navigation error, which constitutes the majority of the tracking error. Given the uncertainty of navigation solution error, the signal dynamics generated by the navigation solution cannot be optimally tracked using SRUKF-based loop filter with constant parameters.

The steady-state equivalent bandwidth of the KF-based tracking loop is determined by the ratio of the process noise covariance to the measurement noise covariance (**Q**/**R**), and its specific value can be derived from the filter parameters [21]. The Figure 2 illustrates the equivalent noise bandwidth of the KF-based tracking loop in steady-state, considering various process noise covariances **Q**, with respect to the measurement noise covariance **R**. When the signal is weak (i.e., low C/N_0), the loop bandwidth is reduced in order to enhance noise filtering. However, excessively reducing the loop bandwidth may lead to inadequate tracking of dynamic signals during rapid fluctuations. Consequently, adaptive mechanisms are frequently employed to dynamically adjust parameters in real time based on external information, thereby achieving optimal state estimation.

Preprints (www.preprints.org) | NOT PEER-REVIEWED | Posted: 28 December 2023 doi:10.20944/preprints202312.1948.v1

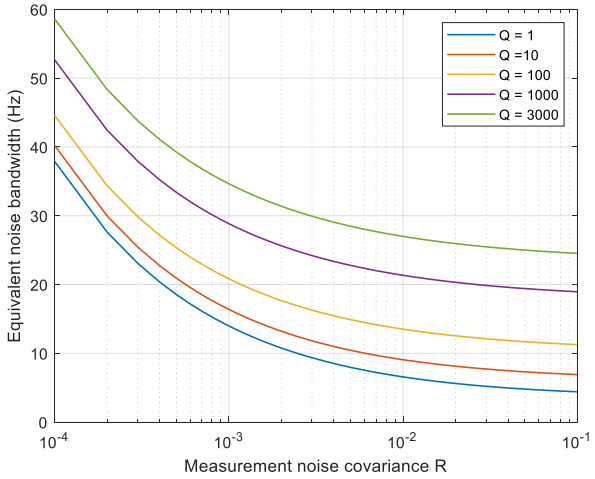

Figure 2. Equivalent noise bandwidth of the KF-based tracking loop in steady-state.

Table 1. Procedures of the SRUKF.

Algorithm. SRUKF algorithm for tracking loop

Initialization:

$$\hat{\mathbf{X}}_0 = E(\mathbf{X}_0), \mathbf{S}_0 = chol\left(E\left[\left(\mathbf{X}_0 - \hat{\mathbf{X}}_0 \right)\left(\mathbf{X}_0 - \hat{\mathbf{X}}_0 \right)^T \right] \right)$$

for $k = 1 : end$

Calculate sigma point:

$$\xi_{k-1} = \left[\hat{\mathbf{X}}_{k-1} \quad \hat{\mathbf{X}}_{k-1} + \sqrt{n+\lambda}\left(\mathbf{S}_{x_{k-1}} \right)_i \quad \hat{\mathbf{X}}_{k-1} - \sqrt{n+\lambda}\left(\mathbf{S}_{x_{k-1}} \right)_i \right], i = 1, \cdots, n$$

Time update:

$$\xi_{i,k|k-1} = f\left(\xi_{i,k-1} \right), i = 0,1, \cdots, n$$

$$\hat{\mathbf{X}}_{k|k-1} = \sum_{i=0}^{2n} W_i^m \xi_{i,k|k-1}$$

QR decomposition: $\mathbf{S}_{x_{k|k-1}} = qr\left[\sqrt{W_{1:2n}^c}\left(\xi_{1:2n,k|k-1} - \hat{\mathbf{X}}_{k|k-1} \right) \quad \sqrt{\mathbf{Q}_k} \right]$

Cholesky factor updating: $\mathbf{S}_{x_{k|k-1}} = cholupdate\left[\mathbf{S}_{x_{k|k-1}}, \sqrt{\left| W_0^c \right|}\left(\xi_{0,k|k-1} - \hat{\mathbf{X}}_{k|k-1} \right), -1 \right]$

Calculate the sigma points again, and measurement update:

$$\xi_{k,k-1} = \left[\hat{\mathbf{X}}_{k,k-1} \quad \hat{\mathbf{X}}_{k,k-1} + \sqrt{n+\lambda}\left(\mathbf{S}_{x_{k,k-1}} \right)_i \quad \hat{\mathbf{X}}_{k,k-1} - \sqrt{n+\lambda}\left(\mathbf{S}_{x_{k,k-1}} \right)_i \right], i = 1, \cdots, n$$

$$\chi_{i,k|k-1} = h\left(\xi_{i,k|k-1} \right), i = 0,1, \cdots, n$$

$$\hat{\mathbf{Z}}_{k|k-1} = \sum_{i=0}^{2n} W_i^m \chi_{i,k|k-1}$$

QR decomposition: $\mathbf{S}_{z_k} = qr\left[\sqrt{W_{1:2n}^c}\left(\chi_{1:2n,k|k-1} - \hat{\mathbf{Z}}_{k|k-1} \right) \quad \sqrt{R_k} \right]$

Cholesky factor updating: $\mathbf{S}_{z_k} = cholupdate\left[\mathbf{S}_{z_k}, \sqrt{\left| W_0^c \right|}\left(\chi_{0,k|k-1} - \hat{\mathbf{Z}}_{k|k-1} \right), -1 \right]$

$$\mathbf{P}_{xz,k|k-1} = \sum_{i=0}^{2n} W_i^c \left[\xi_{i,k|k-1} - \hat{\mathbf{X}}_{k|k-1} \right]\left[\chi_{i,k|k-1} - \hat{\mathbf{Z}}_{k|k-1} \right]^T$$

Filter update:

$$\mathbf{K}_k = \mathbf{P}_{xz,k|k-1}\left(\mathbf{S}_{z_k} \mathbf{S}_{z_k}^T \right)^{-1}$$

$$\hat{\mathbf{X}}_k = \hat{\mathbf{X}}_{k|k-1} + \mathbf{K}_k\left(\mathbf{Z}_k - \hat{\mathbf{Z}}_{k|k-1} \right)$$

$$\mathbf{S}_{x_k} = cholupdate\left[\mathbf{S}_{x_{k|k-1}}, \mathbf{K}_k \mathbf{S}_{z_k}, -1 \right]$$

end

The measurement noise covariance of prompt component in previous studies can be calculated by considering the C/N_0:

Preprints (www.preprints.org) | NOT PEER-REVIEWED | Posted: 28 December 2023 doi:10.20944/preprints202312.1948.v1

$$r_{\eta_{I_P}}^2 = r_{\eta_{Q_P}}^2 = \frac{SP}{2 \bullet 10^{(C/N_0)/10} \bullet T_{coh}} \tag{15}$$

where, η_I and η_Q can be referred to the description in the Equation **Error! Reference source not found.**. The signal power is denoted as $SP = A^2/2$, while the C/N_0 is expressed in units of *dBHz*. The narrowband broadband power ratio method (NWPR) is employed in this paper for calculating the C/N_0 due to its superior estimation performance when dealing with weak signals.

In addition, the noise covariance of the early and late branches is calculated as follows:

$$r_{\eta_{I_E}}^2 = r_{\eta_{Q_E}}^2 = r_{\eta_{I_L}}^2 = r_{\eta_{Q_L}}^2 = R(d) r_{\eta_{I_P}}^2 \tag{16}$$

Thus, corresponding to Equation **Error! Reference source not found.**, the measurement noise covariance matrix $\mathbf{R}_k$ of the loop filter is represented as a diagonal matrix in the following form:

$$\mathbf{R}_k = diag\left[r_{\eta_{I_P}}^2 \quad r_{\eta_{I_E}}^2 \quad r_{\eta_{I_L}}^2 \quad r_{\eta_{Q_P}}^2 \quad r_{\eta_{Q_E}}^2 \quad r_{\eta_{Q_L}}^2 \right] \tag{17}$$

However, the determination of dynamic stress in the tracking loop solely based on C/N_0 is insufficient. Therefore, this research also considers adaptive adjustment of process noise covariance $\mathbf{Q}_k$, which can be modified based on estimated Doppler frequency error resulting from the uncertainty of the navigation solution. Essentially, the imprecision associated with navigation error manifests the dynamics of the tracking loop, which resulting in an inherent uncertainty in the state equation.

Primarily, in accordance with Equation **Error! Reference source not found.**, the uncertainty of the estimated Doppler frequency is determined through the examination of the state covariance during the navigation solution process.

$$\sigma_{aid,k}^2 = \left[\mathbf{P}_{d,k} + \mathbf{e}_k^j \cdot \mathbf{P}_{v,k} \cdot \left(\mathbf{e}_k^j \right)^T \right] \cdot \left(\frac{f_{carrier}}{c} \right)^2 \tag{18}$$

where $\mathbf{P}_{d,k}$ and $\mathbf{P}_{v,k}$ represent the noise covariance matrices associated with the clock drift and velocity components, respectively.

Subsequently, the process noise covariance matrix $\mathbf{Q}_k$ of the loop filter is adjusted adaptively based on the Doppler frequency error covariance and thereby effectively regulate the loop noise bandwidth:

$$\hat{\mathbf{Q}}_k = \mathbf{Q}_0 + \Delta \mathbf{Q}_k \tag{19}$$

where, $\mathbf{Q}_0$ signifies the initial value of state noise covariance, with the setting criteria available in reference 22. Additionally, $\Delta \mathbf{Q}_k$ represents the additional process noise covariance resulting from the uncertainty associated with navigation errors.

$$\Delta \mathbf{Q}_k = \alpha \sqrt{\sigma_{aid,k}^2} \cdot \mathbf{I}_Q \tag{20}$$

where, α represents the scale factor governing the conversion from Doppler frequency error to process noise covariance, while $\mathbf{I}_Q$ is the identity matrix of the same dimension as $\mathbf{Q}_k$. It is worth noting that α determines the sensitivity of the $\Delta \mathbf{Q}_k$ matrix concerning Doppler frequency error. Therefore, α can adjust itself according to C/N_0 :

$$\alpha = \frac{\alpha_0}{C/N_0} \tag{21}$$

Preprints (www.preprints.org) | NOT PEER-REVIEWED | Posted: 28 December 2023 doi:10.20944/preprints202312.1948.v1

It becomes evident that inverse proportionality between the sensitivity of matrix $\Delta\mathbf{Q}_k$ to Doppler frequency error and C/N_0. The sensitivity of the Doppler error can be appropriately reduced when the C/N_0 is high, while a decrease in C/N_0 results in heightened sensitivity.

4. Experimental Evaluation and Results

4.1. Experimental Setup

The efficacy of the proposed method underwent evaluation through the establishment of a vehicle verification platform, depicted in Figure 3. The Trimble BD992 receiver are employed to deliver accurate position and velocity references. Operating in fixed RTK mode, the receiver demonstrated outstanding horizontal positioning accuracy of 0.8 cm and vertical positioning accuracy of 1.5 cm. The Gstar UTREK-210 IF signal collector is employed for the collection of the satellite's IF signal, with the IF $f_{IF} = 4.5MHz$ and sampling rate $f_s = 19.1999MHz$. The two devices are interconnected through a power splitter, enabling them to share the same satellite antenna installed on the vehicle's rooftop.

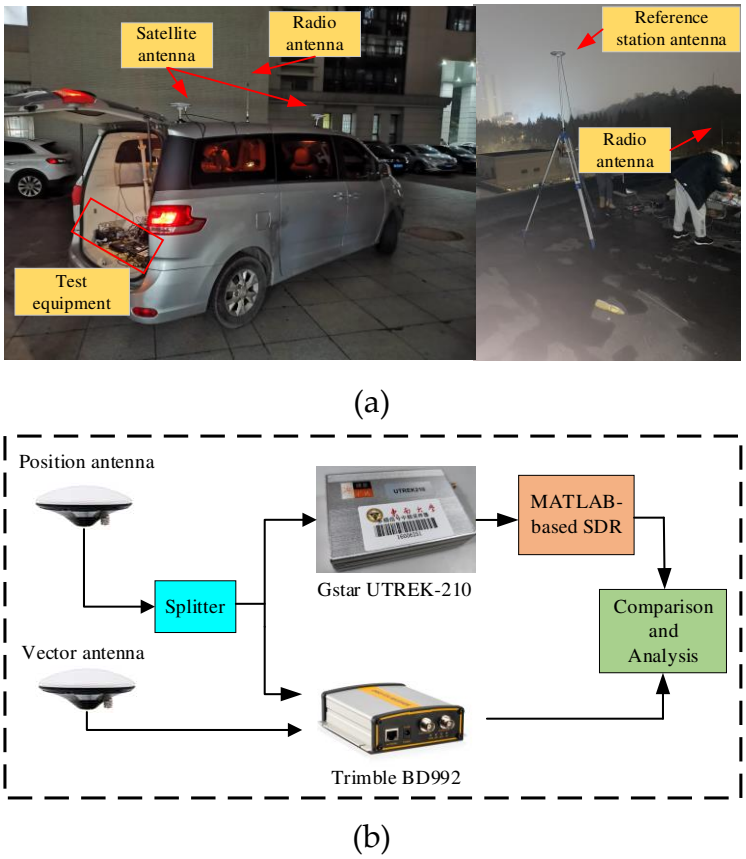

Figure 3. (a) Experiment equipment and (b) performance evaluation method.

The MATLAB-based GPS L1 SDR was used to evaluate the receiver performance of various methods. This research encompasses the evaluation of four distinct SDR architectures, which include:

Scheme 1: Scalar tracking receivers based on conventional tracking loops (CTL-based STL);
Scheme 2: Vector tracking receiver based on EKF loop filter (EKF-based VTL);
Scheme 3: Vector tracking receiver based on SRUKF loop filter (UKF-based VTL);
Scheme 4: Vector tracking receiver based on ASRUKF loop filter (ASRUKF-based VTL).
The parameter configurations specific to the aforementioned methods are presented in Table 2.

Table 2. Parameter configurations of comparison scheme.

Preprints (www.preprints.org) | NOT PEER-REVIEWED | Posted: 28 December 2023 doi:10.20944/preprints202312.1948.v1

Special parameter	Value
Correlator interval d	0.5 chip
DLL noise bandwidth	1 Hz
PLL noise bandwidth	10 Hz
Coherence integration time T_{coh}	1 ms
Navigation filter update time T_{nav}	100 ms

4.2. Tracking Performance Analysis

The vehicle experiment was conducted on the city road in Nanjing, China. The experimental environment encompasses various elements such as open sky, high buildings and trees, and other natural settings. The driving maneuvers encompassed acceleration, deceleration, and turning maneuvers. The data collection is scheduled to commence at UTC 11:28:46, December 18, 2021, with a designated analysis period of 200 seconds. There are six satellites were acquired successfully in the course of the experiment. The satellite sky-plot is displayed in Figure 4, with an average Position Dilution of Precision (PDOP) value of 2.2975.

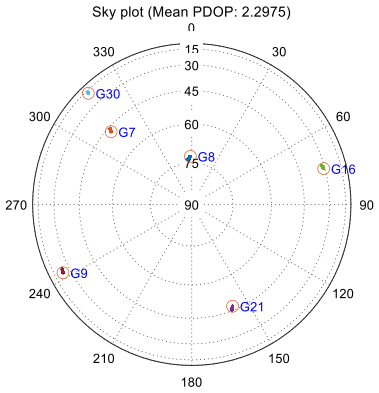

Figure 4. Sky-Plot of the acquired satellites and the mean PDOP value.

The C/N_0 of all satellites throughout the entire experiment is illustrated in Figure 4. It is apparent that the C/N_0 remains relatively stable during vehicle operation; however, certain satellite signals exhibit a more significant decline when encountering severe interference or occlusion. This significantly impacts the continuity of the tracking loop, potentially leading to inaccuracies in positioning results.

A closer look at Figure 5 reveals that, owing to the low elevation angle of satellite G16, the signal experiences severe blockage is in motion around 150 seconds, leading to a sharp decline in the C/N_0 and significantly impacting the tracking loop. Illustrated in Figure 6a, the Doppler frequency estimation of the conventional STL is notably affected within the corresponding signal interruption interval. However, the VTL can combine all the channel information and utilizes the navigation information calculated by the navigation solution module to estimate the carrier frequency. This enables continuous tracking even under short periods of signal interruption.

Preprints (www.preprints.org) | NOT PEER-REVIEWED | Posted: 28 December 2023 doi:10.20944/preprints202312.1948.v1

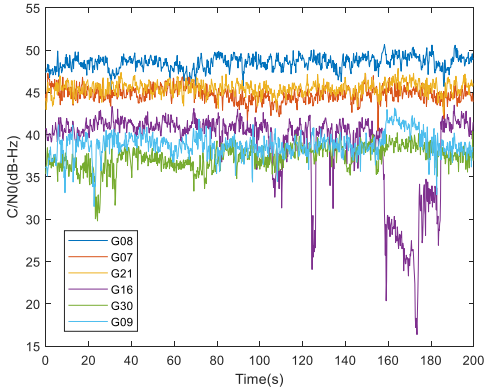

Figure 5. of all satellites during the test.

In addition, phase lock indicator (PLI) serves as a metric to evaluate the tracking performance of each method, and the closer the PLI value is to 1, the higher the tracking accuracy [33]. It can be clearly seen from Figure 6b that the independence of each channel in traditional scalar tracking has a significant impact on the tracking performance of the single loop when influenced by external factors. In contrast, the VTL facilitates mutual assistance between channels, thereby enhancing tracking accuracy even when a single channel is disturbed.

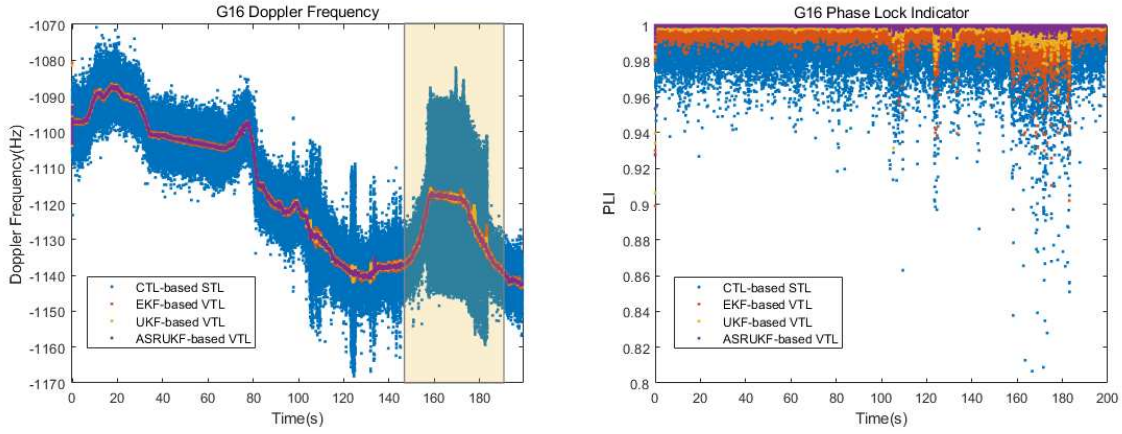

(a) (b)

Figure 6. (a) Doppler frequency estimation and (b) PLIs of G16 of both schemes.

4.3. PVT Results Evaluation

In addition, we utilize the navigation results generated by the high-precision Trimble RTK receiver as a benchmark to evaluate the position and velocity accuracy of the proposed method. The PVT results are crucial in determining the performance of the receiver, and their precision also impacts the accuracy of feedback Doppler frequency information, which indirectly influences loop tracking performance.

The position errors of different methods are illustrated in Figure 7, revealing that the VTL based on KF loop significantly improve the positioning accuracy compared to the STL receiver using the CTL. Especially when the signal is occluded (150s-180s data segment), all methods are affected. However, the VTL method, by combining feedback information calculated by all channels, effectively shares information between channels, leading to improved positioning accuracy in interference environments. Among these methods, the VTL method based on ASRUKF demonstrates the highest level of accuracy, followed by the VTL method based on UKF, while the VTL method based on EKF exhibits comparatively lower performance. This demonstrates the superior efficacy of UKF over EKF

Preprints (www.preprints.org) | NOT PEER-REVIEWED | Posted: 28 December 2023 doi:10.20944/preprints202312.1948.v1

in nonlinear approximation. Furthermore, by incorporating a parameter adaptation method, ASRUKF dynamically adjusts the UKF bandwidth in real time based on the dynamics of the vehicle, so as to obtain more stable navigation and positioning results.

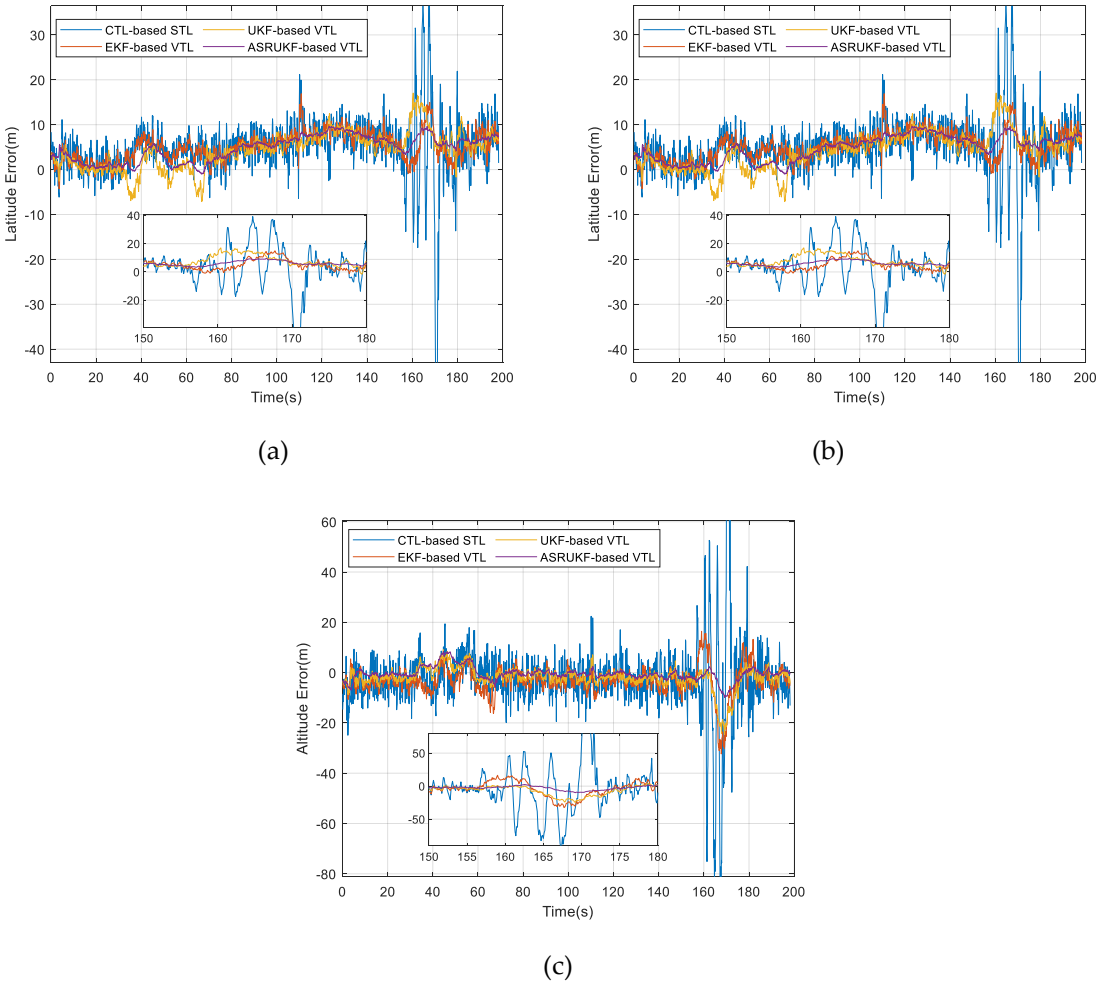

Figure 7. (a)Latitude errors, (b)longitude errors and (c) altitude errors of both schemes.

The root mean square error (RMSE) and standard deviation (STD) of position in three directions are summarized in Table 3. The table clearly demonstrates a significant enhancement in the accuracy of EKF-based VTL compared to CTL-based STL. Moreover, the advantages of UKF-based VTL and ASRUKF-based VTL have been convincingly demonstrated.

Table 3. Positioning errors of the different schemes.

Method	Latitude Error (m)		Longitude Error (m)		Altitude Error (m)	
	RMSE	STD	RMSE	STD	RMSE	STD
CTL-based STL	8.54	7.12	8.72	8.72	17.16	17.02
EKF-based VTL	5.94	3.08	4.07	4.06	6.57	5.75
UKF-based VTL	5.84	4.07	3.46	3.46	4.81	4.36
ASRUKF-based VTL	5.48	2.79	2.34	2.25	2.69	2.65

Furthermore, Figure 8 and Table 4 present the results of velocity error and their corresponding statistics, respectively, showing the same conclusion as the positions. The observation from Figure 8 reveals that, during the vehicle driving process, ASRUKF-based VTL adaptively adjusts the measurement noise covariance matrix **R** and process noise covariance **Q** respectively according to the signal C/N_0 and feedback Doppler error. This adaptive adjustment optimizes the noise

Preprints (www.preprints.org) | NOT PEER-REVIEWED | Posted: 28 December 2023 doi:10.20944/preprints202312.1948.v1

bandwidth, facilitating more effective tracking of dynamic signals. The experimental results prove that the proposed method achieves PVT outcomes with enhanced precision, thus improving the robustness and accuracy of the receiver in complex environments.

Table 4. Velocity errors of the different schemes.

Method	East Velocity Error (m/s)		North Velocity Error (m/s)	
	RMSE	STD	RMSE	STD
CTL-based STL	0.48	0.48	0.45	0.45
EKF-based VTL	0.16	0.15	0.22	0.22
UKF-based VTL	0.14	0.15	0.22	0.21
ASRUKF-based VTL	0.13	0.14	0.20	0.20

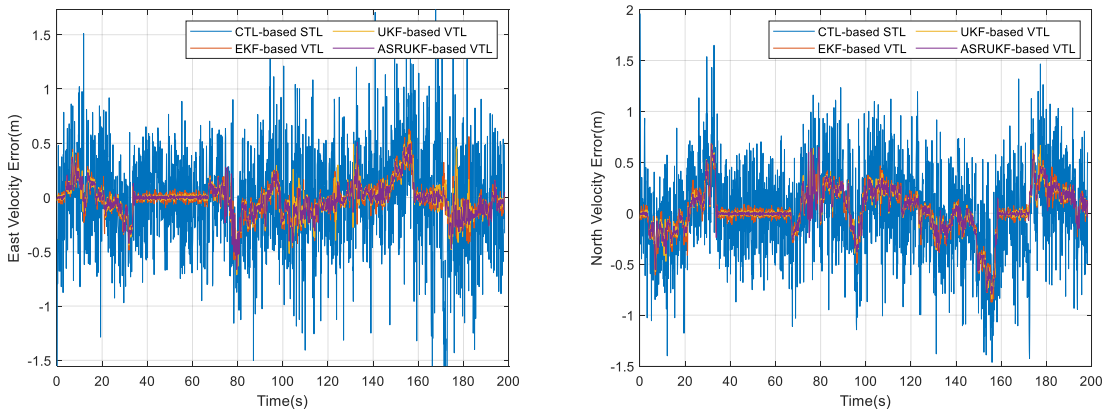

(a) (b)

Figure 8. The velocity error in the (a) east and (b) north direction for both schemes.

5. Conclusion

The paper introduces a vector tracking receive based on a nonlinear Kalman Filter (KF) tracking loop to enhance the receiver's performance in complex environments. Firstly, the structure of the VTL is described in detail. Secondly, to address the strong nonlinearity arising from the loop filter using I/Q information as the measurement, the UKF is employed instead of the EKF to avoid the truncation errors associated with the first-order approximation. Additionally, square root filtering and adaptive criteria are introduced. ASRUKF dynamically adjusts the noise bandwidth based on the signal C/N_0 and feedback error, thereby improving the stability and robustness of the tracking loop. Finally, a field vehicle experiment is designed, and the results of SDR based on different structures are compared, demonstrating the superiority of the proposed method in complex dynamic environments.

In addition, the successful implementation of the proposed method provides a way to introduce other sensors to assist the receiver loop tracking and improve GNSS receiver dynamic range and robustness, such as GNSS/INS ultra-tight integration.

Author Contributions: Conceptualization, N.G. and Z.Y.; methodology, N.G.; software, N.G.; validation, N.G.; formal analysis, N.G.; investigation, N.G.; resources, X.C.; data curation, N.G.; writing—original draft preparation, N.G.; writing—review and editing, N.G. and Z.J.; visualization, N.G.; supervision, X.C.; project administration, X.C.; funding acquisition, X.C. All authors have read and agreed to the published version of the manuscript.

Funding: This research was funded by National Natural Science Foundation of China, grant number No. 61873064.

Data Availability Statement: The data presented in this study are available on request from the corresponding author. The data are not publicly available due to privacy.

Acknowledgments: The authors would like to thank Yulu Zhong and Junwei Wang for their assistance in the completion of experiments.

Conflicts of Interest: The authors declare no conflicts of interest.

References

1. Locubiche-Serra, S.; Seco-Granados, G.; López-Salcedo, J. A. Performance assessment of a low-complexity autoregressive Kalman filter for GNSS carrier tracking using real scintillation time series. *GPS Solut.* **2022**, 26, 1-14.
2. Jiang, C.; Chen, S.; Chen, Y.; Liu, D.; Bo, Y. GNSS vector tracking method using graph optimization. *IEEE Trans. Circuits Syst. II-Express Briefs* **2020**, 68, 1313-1317.
3. Yan, Z.; Ruotsalainen, L.; Chen, X.; Tang, X. An INS-assisted vector tracking receiver with multipath error estimation for dense urban canyons[J]. *GPS Solut.* **2023**, 27, 88.
4. Peng, Z.; Gao, Y.; Gao, C.; Shang, R.; Gan, L. Improving Smartphone GNSS Positioning Accuracy Using Inequality Constraints. *Remote Sens.* **2023**, 15, 2062.
5. Ding, Y.; Chauchat, P.; Pages, G.; Asseman, P. Learning-enhanced adaptive robust GNSS navigation in challenging environments. *IEEE Robot. Autom. Lett.* **2022**, 7(4): 9905-9912.
6. Shen, C.; Zhao, X.; Wu, X.; Cao, H.; Wang, C.; Tang, J.; Liu, J. Multi-aperture Visual Velocity Measurement Method based on Biomimetic Compound-eye for UAVs. *IEEE Internet Things J.* **2023**.
7. Jiang, C.; Chen, Y.; Xu, B.; Jia, J.; Sun, H.; Chen, C.; Zhiyong Duan; Yuming Bo Hyyppä, J. Vector tracking based on factor graph optimization for GNSS NLOS bias estimation and correction. *IEEE Internet Things J.* **2022**, 9, 16209-16221.
8. Lashley, M.; Bevly, D, M.; Hung, J, Y. Performance analysis of vector tracking algorithms for weak GPS signals in high dynamics. *IEEE J. Sel. Top. Signal Process.* **2009**, 3, 661-673.
9. Yan, Z.; Chen, X.; Tang, X.; Zhu, X. Design and Performance Evaluation of the Improved INS-Assisted Vector Tracking for the Multipath in Urban Canyons. *IEEE Trans. Instrum. Meas.* **2022**, *71*, 1-16.
10. Zhao, S.; Akos, D. An open source GPS/GNSS vector tracking loop-implementation, filter tuning, and results. In Proceedings of the 2011 International Technical Meeting of The Institute of Navigation (ITM), San Diego, California, USA 24-26, Jan 2011; pp.1293-1305.
11. Xu, B.; Hsu, L, T. Open-source MATLAB code for GPS vector tracking on a software-defined receiver. *GPS Solut*. **2019**, 23, 1-9.
12. GEBRE-EGZIABHER, D. E. M. O. Z.; Razavi, A.; Enge, P. K.; Gautier, J.; Pullen, S.; Pervan, B. S.; Akos, D. M. Sensitivity and Performance Analysis of Doppler-Aided GPS Carrier-Tracking Loops. *Navigation*, 2005, 52, 49-60.
13. Zhang, T.; Zhang, H.; Lin, T.; Yan, K.; Niu, X. Modeling and verifying the impact of time delay on INS-aided GNSS PLLs. *GPS Solut*. **2016**, 20, 725-736.
14. Cheng, Y.; Chang, Q. A carrier tracking loop using adaptive strong tracking Kalman filter in GNSS receivers. *IEEE Commun. Lett.* **2020**, 24, 2903-2907.
15. Yang, H.; Zhou, B.; Wang, L.; Wei, Q.; Ji, F.; Zhang, R. Performance and evaluation of GNSS receiver vector tracking loop based on adaptive cascade filter. *Remote Sens.* **2021**, 13, 1477.
16. Wu, M.; Zhao, L.; Ding, J.; Gao, Y.; Li, Y.; Kang, Y. A BDS-3 B1C/B2a dual-frequency joint tracking architecture based on adaptive Kalman filter and extended integration time. *GPS Solut*. **2020**, 24, 1-16.
17. Sun. D.; Petovello, M, G.; Cannon, M, E. Use of a reduced IMU to aid a GPS receiver with adaptive tracking loops for land vehicle navigation. *GPS Solut*. **2010**, 14, 319-329.
18. Cortés, I.; van der Merwe, J. R.; Lohan, E. S.; Nurmi, J.; Felber, W. Performance evaluation of adaptive tracking techniques with direct-state Kalman filter. *Sensors*, **2022**, 22, 420.
19. Jin T, Wang C, Lu X, et al. Analysis of a federal Kalman filter-based tracking loop for GPS signals. *GPS Solut.* **2019**, 23, 1-13.
20. Klokov, A.; Kanouj, M.; Mironchev, A. A novel carrier tracking approach for GPS signals based on Gauss–Hermite Kalman filter. *Electronics*, **2022**, 11, 2215.
21. Tang X.; Wang, C.; Lu, X.; Ling, K. V.; Cong, L. The explicit tuning investigation and validation of a full Kalman filter-based tracking loop in GNSS receivers. IEEE Access, 2019, 7: 111487-111498.
22. Tang, X.; Falco, G.; Falletti, E.; Lo Presti, L. Theoretical analysis and tuning criteria of the Kalman filter-based tracking loop. *GPS Solut.* **2015**, 19, 489-503.
23. Miao, Z. Y.; Lv, Y. L.; Xu, D. J.; Shen, F.; Pang, S. W. Analysis of a variational Bayesian adaptive cubature Kalman filter tracking loop for high dynamic conditions. *GPS Solut.* **2017**, 21, 111-122.
24. Cortés, I.; Conde, N.; Van Der Merwe, J. R.; Lohan, E. S.; Nurmi, J.; Felber, W. Low-complexity adaptive direct-state Kalman filter for robust GNSS carrier tracking. In 2022 International Conference on Localization and GNSS (ICL-GNSS). Tampere, Finland, 7-9 Jun 2022; pp. 1-7.

25. Tang, X.; Falco, G.; Falletti, E.; Presti, L. L. Practical implementation and performance assessment of an Extended Kalman Filter-based signal tracking loop. In 2013 International Conference on Localization and GNSS (ICL-GNSS). Turin, Italy,25-27 Jun 2013; pp. 139-144.
26. Zeng, C.; Li, W. Application of extended Kalman filter for tracking high dynamic GPS signal. In 2016 IEEE International Conference on Signal and Image Processing (ICSIP). Beijing, China, 13-15 Aug 2016; pp. 503-507.
27. Tu, Z.; Lou, Y.; Guo, W.; Song, W.; Wang, Y. Design and Validation of a Cascading Vector Tracking Loop in High Dynamic Environments. *Remote Sens.* **2021**, 13, 2000.
28. Liu, J.; Chen, X.; Wang, J. Strong Tracking UKF-Based Hybrid Algorithm and Its Application to Initial Alignment of Rotating SINS With Large Misalignment Angles. *IEEE Trans. Ind. Electron.* **2022**, 70, 8334-8343.
29. Zhong, Y.; Chen, X.; Zhou, Y.; Wang, J. Adaptive Particle Filtering with Variational Bayesian and Its Application for INS/GPS Integrated Navigation. *IEEE Sens. J.* **2023**.
30. Gao, Z.; Mu, D.; Gao, S.; Zhong, Y.; Gu, C. Adaptive unscented Kalman filter based on maximum posterior and random weighting. *Aerosp. Sci. Technol*. **2017**, 71, 12-24.
31. Jwo, D. J.; Yang, C. F.; Chuang, C. H.; Lee, T. Y. Performance enhancement for ultra-tight GPS/INS integration using a fuzzy adaptive strong tracking unscented Kalman filter. *Nonlinear Dyn*. **2013**, 73, 377-395.
32. Zhang, T.; Shi, J.; Lin, T.; Feng, X.; Niu, X. GNSS position-aided delay-locked loops for accurate urban navigation. *GPS Solut.* **2023**, 27, 1-15.
33. Chen, S.; Gao, Y. Improvement of carrier phase tracking in high dynamics conditions using an adaptive joint vector tracking architecture. *GPS Solut.* **2019**, 23, 15.